Multilayer Films for Figured X-Ray Optics

David L. Windt
Bell Labs, Lucent Technologies, Room 1D-456, 600 Mountain Ave., Murray Hill, NJ 07974
windt@bell-labs.com • www.bell-labs.com/user/windt

ABSTRACT

High reflectance multilayer films can now be deposited onto figured substrates to make focusing X-ray mirrors. In this paper, I discuss a variety of topics associated with the development and further refinement of such X-ray optics: high-efficiency multilayer films for use near normal incidence in the 170-300 Å region; depth-graded multilayer films for broad-band reflectance in the 10-100 keV region; surface roughness and it's effect on mirror performance; and finally stresses in multilayer films.

1. INTRODUCTION

The difficulty in producing efficient X-ray optics is due primarily to the fact that at incidence angles much larger than the critical angle for total external reflection, the X-ray reflectance at the interface between any two materials is exceedingly low, perhaps one part in 1000 or even much less. In recent years, however, this problem has been partially circumvented by the development of multilayer thin films: in such structures, a stack of layers - or a stack of interfaces, really - is arranged such that the reflections from each interface add in phase, giving rise to high reflectance over a limited range of incidence angles and photon wavelengths.

Reflective multilayer films can now be deposited onto flat and figured substrates to produce highly efficient X-ray mirrors; multilayer coated reflection gratings and beamsplitters can be produced as well. The development of such multilayer optics has in turn enabled a variety of new and exciting applications in such diverse fields as solar and astrophysics, instrumentation for synchrotron radiation and plasma physics diagnostics, and photo-lithography.

I present below a brief description of some recent activities directed at the development and further refinement of figured multilayer X-ray optics. Unlike a general review article, the material presented here is certainly biased towards my own research: I thus describe in section 2 the development of periodic multilayer films for use near normal incidence in the λ=170 - 300 Å region, primarily for solar physics applications; I describe in section 3 the development of depth-graded multilayer films that provide broadband reflectance at grazing incidence from ~10-100 keV, for high-energy astrophysics applications; in section 4 I discuss the effect of substrate roughness on mirror performance; and finally in section 5 I discuss stresses in multilayer films.

2. MULTILAYER FILMS FOR NORMAL INCIDENCE OPTICS

Silicon-based multilayer systems have been developed in recent years that have high normal incidence reflectance at photon wavelengths long-ward of the Si-L edge near 124 Å. This is a wavelength region where the absorption of silicon is low, as can be inferred from the optical constants for silicon[1], shown in Figure 1. The Mo/Si multilayer system is perhaps the most famous of all, providing normal-incidence reflectance approaching 70% just below the Si L-edge, as shown, for example, in Fig. 2(a). The experimental performance of Mo/Si in the range from about 125-200 Å is roughly 85% of the theoretical maximum that would be obtained if it were possible to fabricate these films with perfectly smooth and sharp interfaces. The highest measured reflectances obtained thus correspond to an interface width σ of order 7 Å; this interface width, inferred from the optical performance, correlates well with the average thickness of the amorphous interlayers between the pure Mo and Si layers observed in cross sectional transmission electron microscopy, as shown, for example, in Fig. 2(b). In contrast, the Ru/Si multilayer system shown in Fig. 3 - which should provide high reflectance over a somewhat larger bandwidth relative to

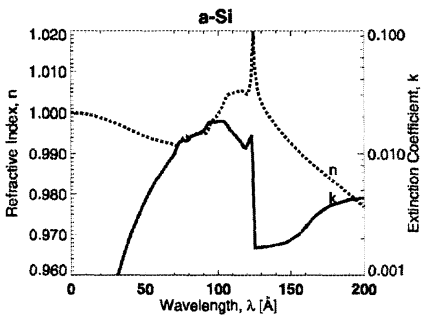

Figure 1 Optical constants of silicon.

Mo/Si - shows performance that is significantly worse than Mo/Si, in both absolute and relative terms, due to the larger amorphous interlayers that form in this system[2].

As a result of the high reflectance and good thermal stability attainable with Mo/Si multilayers, imaging systems using normal-incidence X-ray mirrors coated with this multilayer structure have been developed for a variety of applications, most notably solar physics[3] and extreme ultraviolet lithography[4]. For example, the SoHO solar X-ray telescope[5] made use of periodic Mo/Si multilayers tuned to specific X-ray wavelengths corresponding to coronal emission lines of highly ionized Fe in the range ~170-300 Å; as the abundances of the various ionization states of Fe depend on the equilibrium temperature of the coronal plasma, images of the corona at specific X-ray wavelengths correspond to different coronal temperatures in the range of roughly 600,000 - 2,000,000 degrees. The X-ray mirrors on the recently launched TRACE instrument[6] made use of the same design concept; three of the four quadrants of the telescope mirrors were coated with multilayers tuned to specific X-ray wavelengths: 173 Å (Fe IX/X, $T=10^{5.8}$), 195 Å (Fe XII, $T=10^{6.2}$), and 284 Å (Fe XV, $T=10^{6.3}$). For the TRACE instrument, however, Mo_2C/Si multilayers were used (Fig. 4), which show somewhat better performance than Mo/Si.

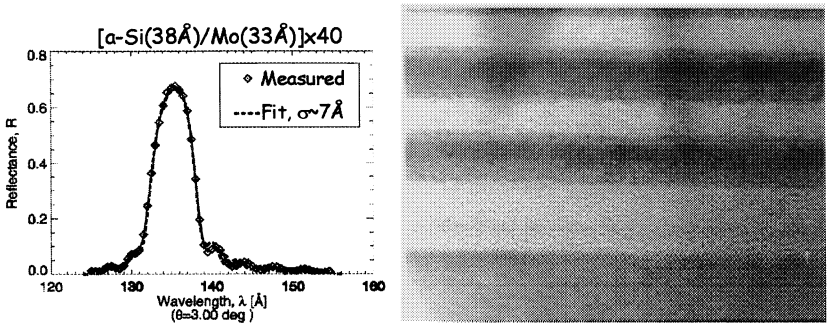

Figure 2 Mo/Si multilayer reflectance (a) and cross-sectional TEM (b).

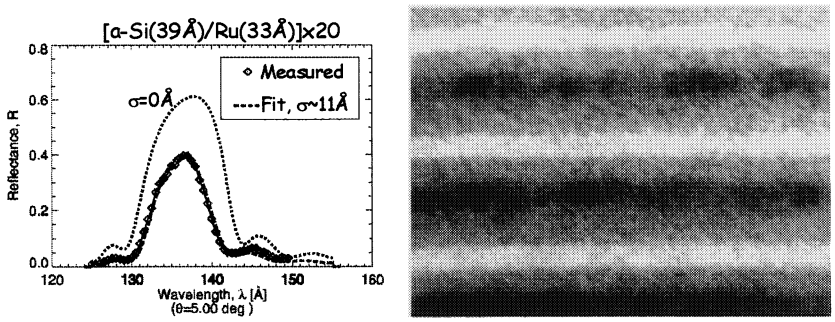

Figure 3. Ru/Si multilayer reflectance (a) and cross-sectional TEM (b).

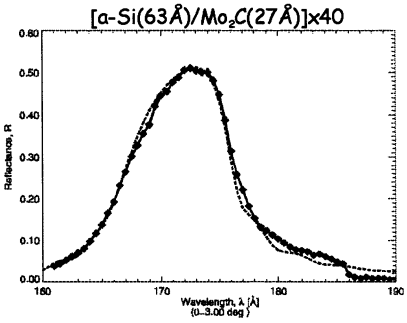

Figure 4. Reflectance of a Mo_2C/Si multilayer.

In principle, aluminum-based multilayers should provide higher normal incidence reflectance than silicon-based multilayers in the 175-300 Å wavelength range, due to the low absorption of aluminum below the L-edge (as can be inferred from the optical constants of Al[1] shown in Fig. 5.) In practice, however, good performance for Al-based multilayers has not yet been realized. For instance, a series of Y/Al, Mo/Al, and Nb/Al multilayers were recently fabricated (by magnetron sputtering,) all of which showed poor optical performance. The highest reflectance was obtained with Y/Al, but the peak reflectance was observed to decay on a time scale of hours, presumably as a result of interdiffusion and/or oxidation. The addition of thin (~3-5Å) amorphous carbon layers between the pure metal layers resulted in essentially no improvement in the case of Mo/Al, but helped significantly in the case of Y/Al: the peak reflectance at λ~190 Å was less than 20% for a simple Y/Al multilayer and greater than 40% for the same period multilayer containing ~3 Å carbon interlayers between each of the metal layers. (A 5 Å carbon capping layer was deposited onto both films.) In spite of this initial improvement, however, the reflectance of the Y/C/Al/C multilayer continued to degrade over a period of weeks, as shown in Fig. 6. Note that the measured reflectance of the as-deposited Y/C/Al/C multilayer film was significantly less than what was expected assuming the optical constants from reference [1], but agreed reasonably well with a reflectance calculation using newly measured optical constants for Y; these new Y optical constants are included in the software described in reference [7], and are shown in Fig. 7.

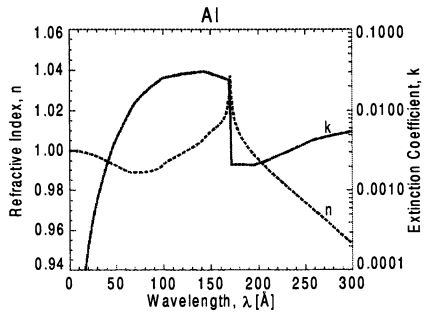

Figure 5. Optical constants of aluminum.

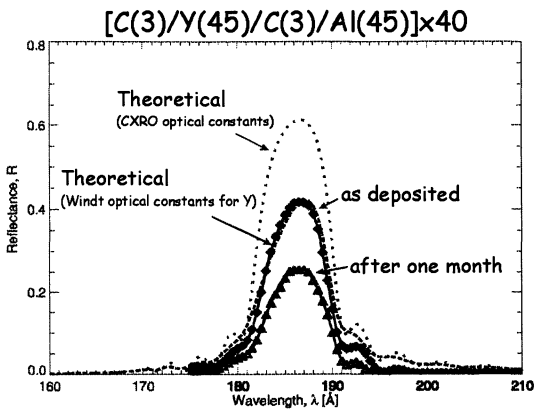

Figure 7. Reflectance of a Y/Al multilayer.

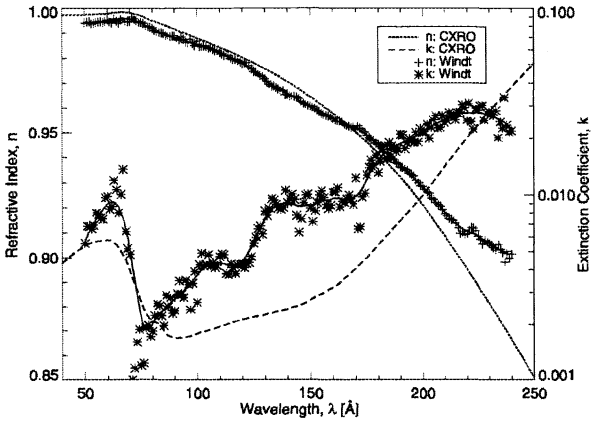

Figure 6. Optical constants for yttrium.

3. DEPTH-GRADED MULTILAYER FILMS FOR GRAZING INCIDENCE OPTICS

As a result of interface imperfections (roughness and diffuseness), the peak reflectance at normal incidence of multilayer films falls rapidly with wavelength. For instance the peak reflectance at λ~45 Å of even the best multilayer film is only of order 5% near normal incidence[8]. At grazing incidence, however, multilayer films still offer a performance advantage over single-layer reflectors at short X-ray wavelengths: a given reflectance can be achieved with a multilayer film at a grazing incidence angle that is several times larger than what can be achieved with a single-layer film at short wavelengths, as illustrated, for example, in Fig 8, which compares the reflectance vs. incidence angle of several periodic W/Si multilayers measured at λ=1.54 Å (8.04 keV) relative to the (theoretical) reflectance of an iridium film. Furthermore, in recent years, depth-graded (aperiodic) multilayer films have been developed[9] that provide broadband grazing incidence reflectance at high energy. In a depth-graded multilayer structure, the bilayer period varies continuously throughout the film stack, so that each bilayer is effectively tuned to a specific wavelength (for a given incidence angle); the overall response of the film can thus be adjusted to provide high reflectance over a wide range of photon energies, simply by adjusting the specific distribution of bilayer thicknesses. In other words, the bandwidth of a depth-graded multilayer film can be optimized for a specific application.

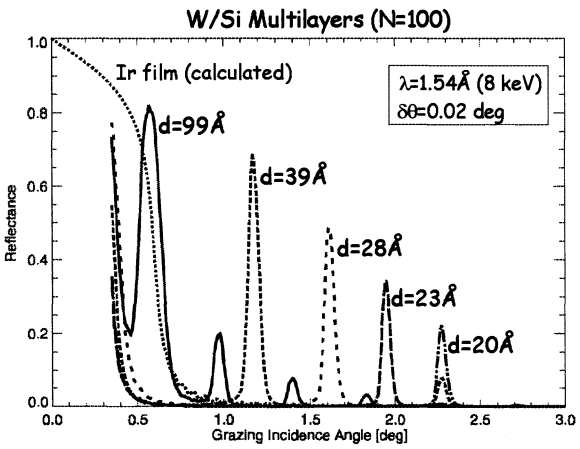

Figure 8. Measured reflectance of W/Si multilayers.

Such depth-graded multilayer structures are now being used to develop, for example, X-ray telescopes for high energy astrophysics that can be used up to energies as high as ~100 keV. For instance, the HEFT (High Energy Focusing Telescope) project[10] is a balloon-borne instrument being developed in a collaboration between Cal Tech, Columbia University, the Danish Space Research Institute, and Bell Labs. The HEFT telescope is an array of 14 telescope modules, and each module is comprised of a nested array of ~80 grazing incidence telescopes, for a total of ~1120 individual telescopes. The individual telescopes, which are divided into quadrants, are made from thin glass sheets that are thermally formed into conic approximations[11] and then coated with depth-graded multilayers. This instrument will provide ~300 sq. cm. of effective area at 40 keV, with sensitivity out to 100 keV.

Recently, in collaboration with P. Mao (Cal Tech,) prototype HEFT telescope mirror quadrants were coated with depth-graded W/Si multilayers prepared by magnetron sputtering. A diagram of the sputtering geometry[12] is shown in Fig. 9. The figured substrate is mounted to a platen that spins at ~200 rpm as it rotates slowly over one or the other magnetron sources, thereby building up the multilayer one layer per pass. The spin motion aids in improving the coating uniformity. The rotational velocity, which is controlled precisely by a computer, is used to adjust the layer thicknesses: assuming that the intrinsic deposition rate of the source is constant, the thickness of a given layer is determined, in principle, by the product of the deposition rate (in Å/sec) and the 'exposure time' (in sec), which is inversely proportional to the rotational velocity of the substrate as it travels over the magnetron source. In practice, however, it was found that the thicknesses of the individual W or Si layers varied in a more complicated way, as will now be described.

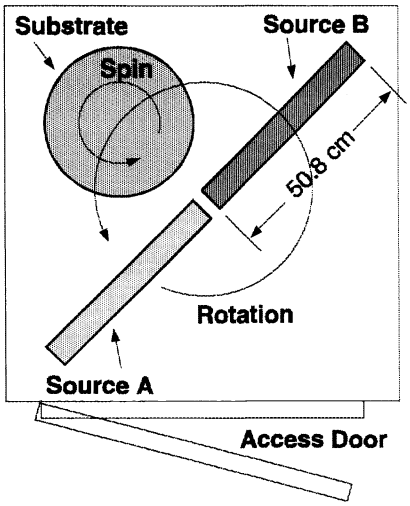

Figure 9. Schematic diagram (top view) of the multilayer sputtering system used to coat figured substrates.

Shown in Fig. 10 are the X-ray reflectance vs. incidence angle curves, measured at 1.54 Å, for a series of periodic W/Si multilayer films (grown under otherwise identical sputtering conditions) in which the multilayer period varied from ~20-200 Å (roughly corresponding to the range of bilayer thicknesses in the depth-graded W/Si multilayers needed for the HEFT mirrors) as a result of variations in the rotational velocities of the substrate. By carefully fitting these curves (dashed lines in Fig. 10,) the relationship between the individual W or Si layer thicknesses was determined as a function of the 'deposition time', that is the exposure time of the substrate to the target during film growth. These relationships are shown separately for W and Si in Figs. 11(a) and 11(b), respectively. In the case of W, the resultant film thickness indeed varies linearly with the exposure time, except that the curve does not go through the origin. The situation is more complicated in the case of Si, where a single linear relationship between film thickness and exposure time does not sufficiently describe the data over the entire range; however, an empirical fit to the

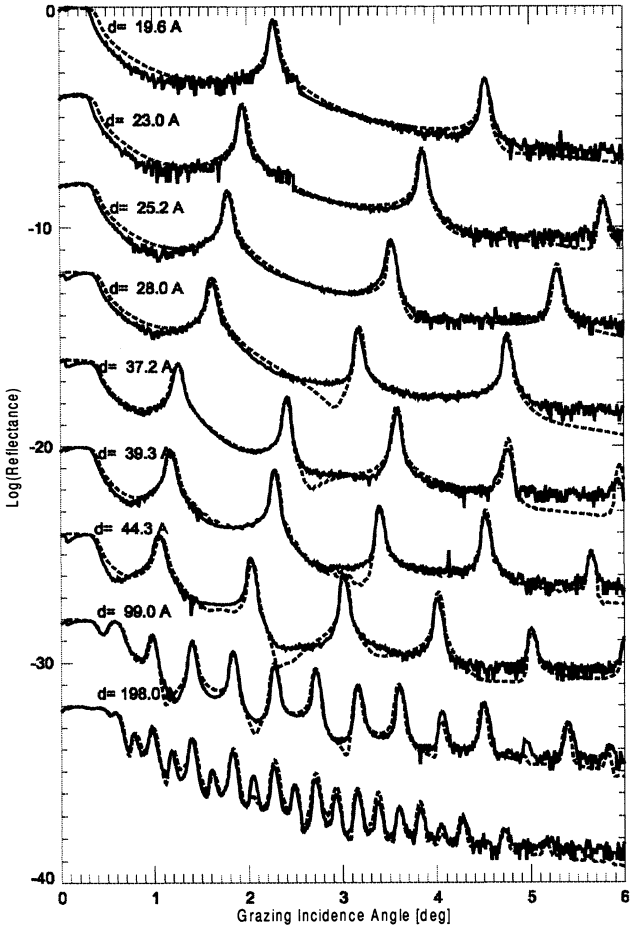

Figure 10. X-ray reflectance of periodic W/Si multilayers.

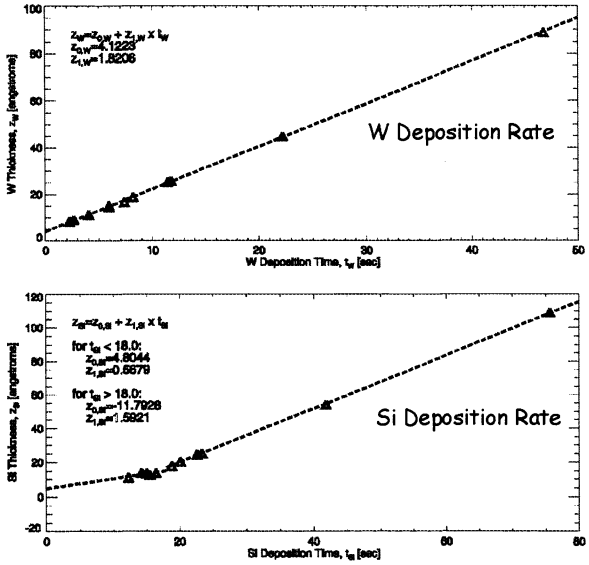

Figure 11. Film thickness vs. exposure time data determined by X-ray reflectance analysis of periodic W/Si multilayers.

data using two separate linear relationships can predict the resultant film thicknesses to within ±1 Å (approx.)

The behavior shown in Fig. 11 can be explained qualitatively in terms of the various processes in competition during film growth: after the deposition of a Si layer, for example, as the substrate passes over the W target, W atoms are deposited onto the Si layer forming a new W layer, but an amorphous W-Si interlayer is forming as well, which results in a reduction in the thicknesses of both the pure W and Si layers; in addition, re-sputtering of Si - i.e., the removal of Si atoms from the growing film as a result of collisions with high energy neutral argon atoms reflected from the W target - will reduce the thickness of the Si layers as well. The effect of these competing processes will vary, in general, with the specific deposition conditions (i.e., Ar pressure, target voltages, target-to-substrate distance, etc.) and should depend on the relative exposure times of W and Si as well.

Nevertheless, using the empirical fits to the deposition rate data shown in Fig. 11, depth-graded W/Si multilayers were grown on both flat and figured substrates. The measured reflectance vs. incidence angle of one such film is shown in Fig. 12, and agrees reasonably well with the expected response. A photo of the coated prototype HEFT mirror segments is shown in Fig. 13. These prototype mirrors are currently being characterized at high energy, and the results of these measurements will be reported elsewhere.

The W/Si graded multilayers just described will work well at energies as high as the W K-edge near 70 keV. To obtain high reflectance out to 100 keV, however, will require a different multilayer structure. To meet this high energy requirement new systems such as Ni/Si and Cu/Si are now being developed. These multilayers work well (theoretically) because the K edges of Ni, Cu and Si are all below the low energy limit (20 keV) of the HEFT telescope mirrors. The grazing incidence X-ray reflectance of typical periodic Ni/Si and Cu/Si periodic multilayers are shown in Figs. 14 and 15. Most promising is the Cu/Si system, for which interface widths of order 2-2.5 Å are inferred from the X-ray reflectance data.

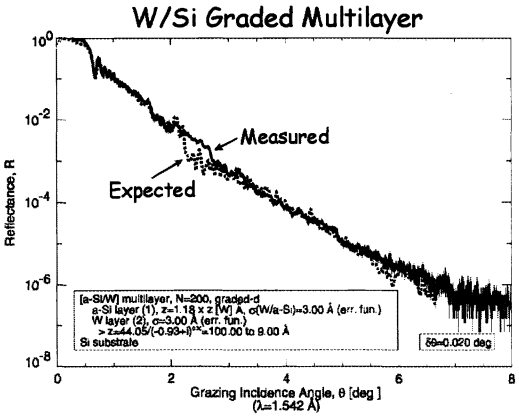

Figure 12. Measured X-ray reflectance of a depth-graded W/Si multilayer film.

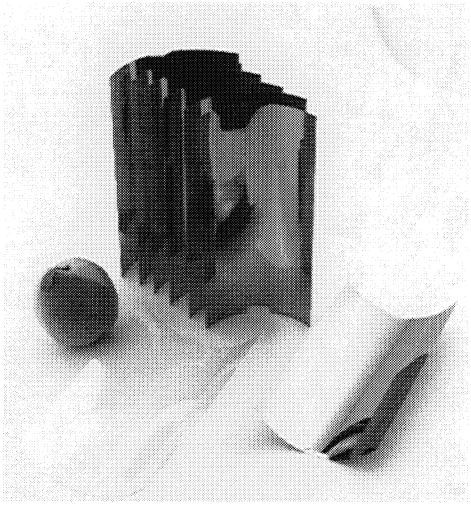

Figure 13. Coated HEFT mirror substrates. A New Jersey peach is shown for scale.

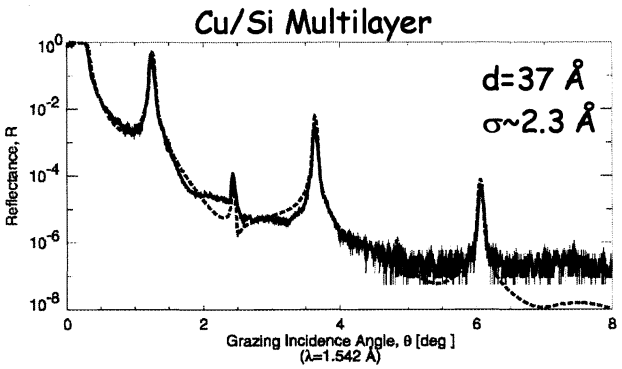

Figure 14. X-ray reflectance of a Cu/Si multilayer.

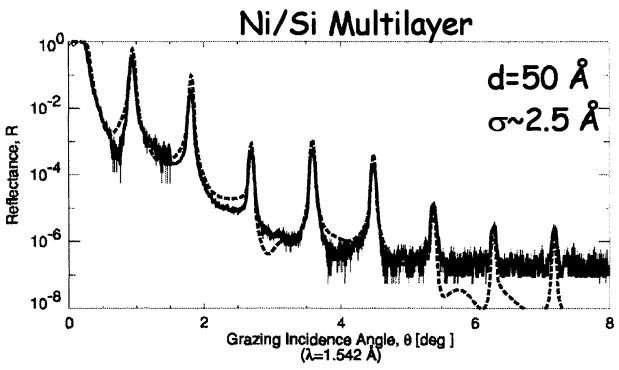

Figure 15. X-ray reflectance of a Ni/Si multilayer.

4. SURFACE FINISH REQUIREMENTS FOR X-RAY OPTICS

Interfacial roughness in a multilayer film has the effect of removing light from the specular direction, thereby reducing the peak reflectance, and scattering that light into non-specular directions. Therefore, in order to produce figured multilayer X-ray mirrors with high reflectance and low scatter it is necessary to control the roughness of the mirror substrate, so that substrate roughness does not propagate up through the multilayer film during growth and degrade the optical performance.

The roughness of a surface or interface can be described in reciprocal space in terms of the so-called Power-Spectral-Density (PSD) function, which is related to the distribution of surface heights (in real space) by a Fourier transform. The two-dimensional PSD function, in units of [length]^4, describes in a sense the distribution of surface roughness as a function of spatial frequency, and in the case of scattering from a single interface, is directly proportional to the distribution of scattered light[13]. For normal incidence mirrors, the largest spatial frequency of interest (i.e., the inverse of the smallest spatial wavelength) is approximately equal to the inverse of the photon wavelength. Thus in the case of X-ray multilayer mirrors for use at normal incidence at a wavelength of order 100 Å, say, it is necessary to measure and control surface roughness on a lateral scale as short as ~100 Å.

Until the development in recent years of scanning probe metrology (e.g., atomic force microscopy), surface roughness measurements were made typically with contact profilers (e.g., Tallystep and Dectac instruments) or with optical interferometers (e.g., WYKO or ZYGO instruments.) Each of these instruments (scanning probe metrology included) measures the surface profile only over a finite range of spatial frequencies. (Only the AFM can probe the high spatial

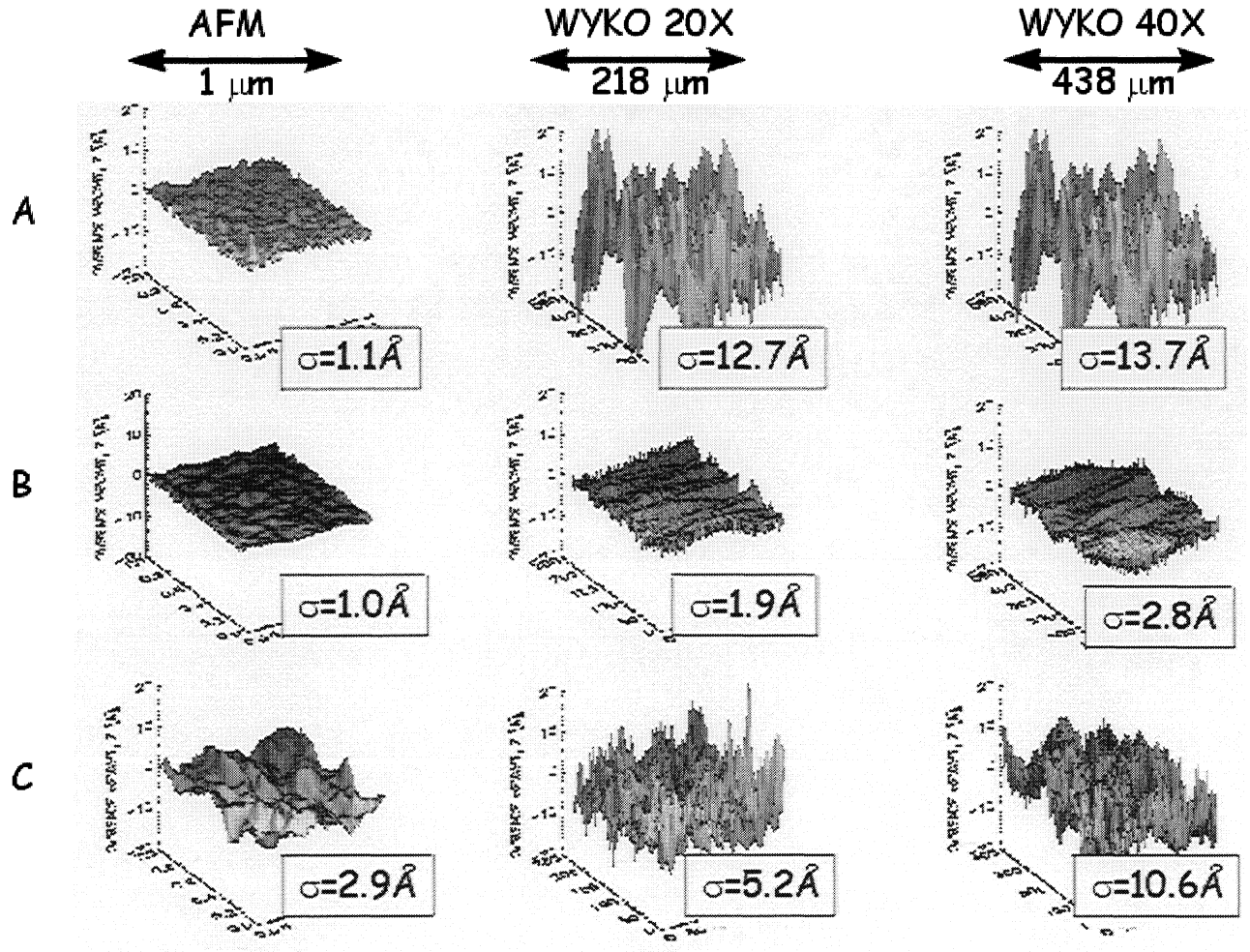

Figure 16. Surface height data for three multilayer coated flats (A, B and C,) as measured with an AFM (left column), and a WYKO TOPO 3D instrument with a 40X mag. objective (center column) and a 20X mag. objective (right column).

frequencies associated with X-ray reflectance losses near normal incidence.) Consequently, the resultant rms surface roughness parameter σ is not a truly intrinsic parameter of the surface, but rather is bandwidth-limited, and is dependent on the range of spatial frequencies probed by the particular instrument used to make the measurement. In other words, the σ value determined by a measurement made with one instrument may be completely uncorrelated with the σ value determined using a different instrument.

As an illustrative example, shown in Fig. 16 are the surface height measurements obtained on three multilayer-coated flats, labeled A, B and C, made using an atomic force microscope (AFM) with a scan length of 1 μm (i.e., sensitivity to spatial wavelengths Λ from ~50 Å-1 μm), and a WYKO TOPO 3D instrument using both a 40X magnification objective and a 20X objective, corresponding to scan lengths of 218 μm (i.e., ~1 < Λ < 218 μm) and 438 μm (i.e., ~2 < Λ < 438 μm), respectively. (Note: a portion of the results described here have been published previously in reference [14].) The rms surface height (σ) values are indicated in the figure: the σ values plainly vary significantly for a given substrate, by more than a factor of 10, in fact, in the case of substrate A. Note, however, that the peak soft X-ray reflectances obtained for these three samples, shown in Fig. 17, are correlated only with the σ values determined from the AFM measurements (as expected,) and are uncorrelated with the WYKO measurements. The PSD functions determined from the AFM data are shown in Fig. 18, and have been fit with an analytic expression of the form[15]

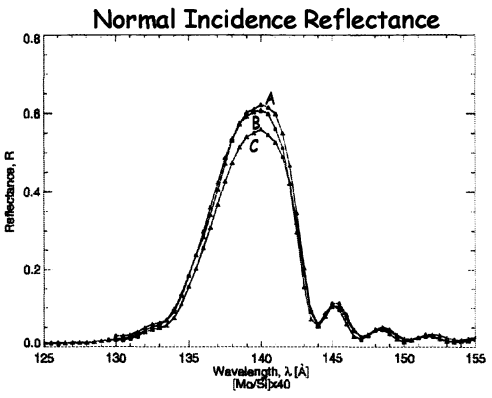

Figure 17. Normal incidence reflectance of the three multilayer-coated flats shown in Fig. 16.

$$S(2\pi f) = \frac{4\pi H \sigma^2 \xi^2}{\left[1 + (2\pi f)^2 \xi^2\right]^{1+H}}.$$

The σ, ξ and H parameters determined from the AFM measurements (indicated in Fig. 18) for the three samples were then used to compute the relative distributions of non-specular reflected intensity using the distorted-wave Born approximation[16]. The computed non-specular reflected intensities are shown in Fig. 19 for the case of rocking scan measurements made at λ=1.45 Å (2θ=1.4 deg), and are in reasonable agreement with the measured values. These measurements thus confirm that high-frequency substrate roughness reduces the specular reflectance of multilayer-coated X-ray mirrors and increases the intensity of diffusely scattered X-rays.

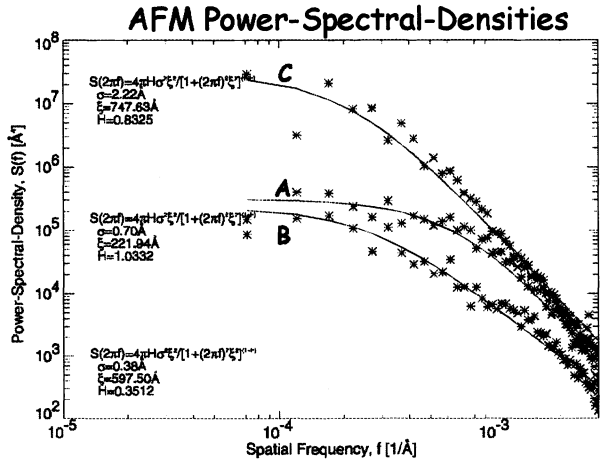

Figure 18. Radially-averaged PSD functions determined from the surface height data shown in Fig. 16.

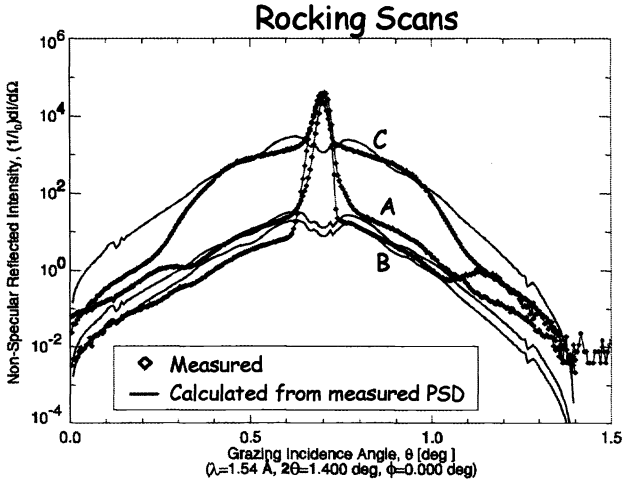

Figure 19. Non-specular reflected intensity data (rocking scans) measured at 1.54 Å for the three samples shown in Figs. 16-18.

5. STRESS CONTROL IN MULTILAYER FILMS

In addition to controlling substrate finish, for high-performance X-ray optical systems it is necessary to control the substrate figure as well. Of particular interest to us now is the fact that large stresses in the multilayer coating might give rise to significant substrate distortions (depending on the substrate thickness and geometry.) As such, it is useful to understand how the net stress in an X-ray multilayer structure depends on the thicknesses of the individual layers as well as on the deposition conditions, in order to develop strategies to minimize the stress in a given film.

The net stress σ_{ML} in a periodic multilayer structure of period d, composed of two types of layers (A and B) having layer thicknesses d_A and d_B, respectively, is equal to the sum of the stresses in the individual A and B layers (σ_A and σ_B) weighted by their relative thicknesses: $\sigma_{ML} d = \sigma_A d_A + \sigma_B d_B + f_{A/B}$, where $f_{A/B}$ is the interface stress (something akin to a surface tension.) So, for example, if the stress in the A layers is compressive while the stress in the B layers is tensile, the net stress of the multilayer can be either compressive or tensile (or zero) depending on the relative layer thicknesses. To complicate matters further, however, the stress in a given layer depends, in general, not just on the deposition conditions (e.g., Ar pressure, target voltage, etc. in the case of sputtered films; substrate temperature, and so forth) but also on the layer thickness itself. That is, in the case of polycrystalline layers, for instance, the microstructure (i.e., grain size, orientation, lattice strain, etc.) - and thus the stress state - of the layer can evolve with film thickness. Consequently, the notion is certainly false that the stress in a multilayer structure made of a particular combination of materials is an intrinsic property of those materials; rather, the stress in a multilayer is an extrinsic property that depends on the deposition conditions and on the relative layer thicknesses. (The *sensitivity* of the stresses in the individual layers to the deposition conditions is no doubt an intrinsic property of the material, however.)

To illustrate, Fig. 20(a) is a plot showing how the stresses measured (by wafer curvature) in Mo/Si multilayer films varies as a function of both Mo and Si layer thickness: each yellow square in this figure corresponds to the stress measured in a periodic multilayer whose Si layer thicknesses are given by the position of the square along the horizontal axis, and whose Mo layer thicknesses are given by the position along the vertical axis. Smooth 'iso-stress' contours were computed using bi-linear interpolation, and are labeled in units of MPa. So, for example, the stress measured for a Mo/Si multilayer containing 3-nm-thick Si layers and 4-nm-thick Mo layers is approximately +300 MPa (tensile). Each of the films used to produce Fig. 20(a) consists of 40 Mo/Si bilayers, and was deposited under otherwise identical deposition conditions.

For the films shown in Fig. 20(a), thinner Mo layers give rise to a more compressive stress state, suggesting that the Si layers are in compression, and the Mo layers in tension. Shown in Fig. 20(b) are the stresses in the same films as measured after one year of storage in air at room temperature; the stresses are measurably different. Figure 20(c) shows the (room temperature) stresses in the same films after a thermal anneal to 300 C (heating at the rate of 20 deg/min.) The change in stress after 300 C anneal (i.e., the final stress minus the as-deposited stress) is shown in Fig. 20(d). The change in stress with thermal cycling can evidently result in either a more compressive or more tensile film, and the magnitude of the stress change can be as large as ~200 MPa, all depending on the specific Mo and Si layer thicknesses.

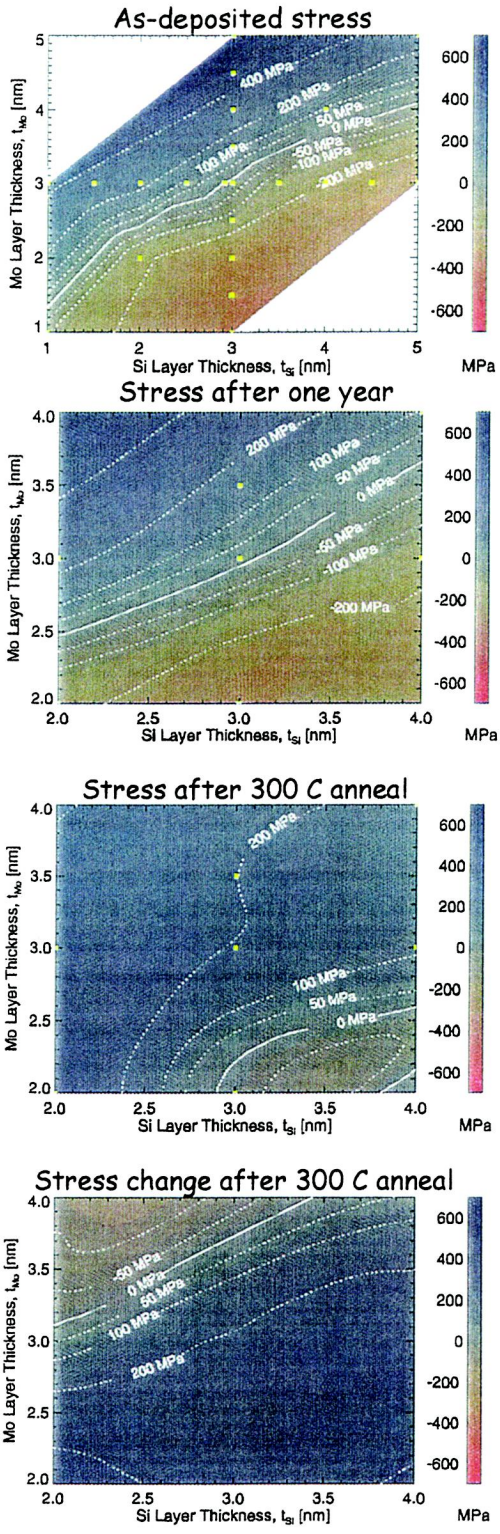

Figure 20. Stresses in Mo/Si multilayers.

Figure 21 shows the large angle X-ray diffraction data (λ=1.54 Å) obtained for some of the Mo/Si multilayers (i.e., those containing 3-nm-thick Si layers) shown in Fig. 20. The peaks near 2θ=40.5° are due to diffraction from the Mo (110) crystallites. Using the Scherrer formula[17] to relate the widths of these peaks to the lateral dimensions of the Mo grains reveals that the lateral grain size is approximately equal to the Mo layer thickness. The variation in the position of the centroid of these peaks also indicates that the strain in the Mo layers depends on both the Mo and Si layer thicknesses. The X-ray data do not reveal any observable change with thermal annealing in either the Mo grain size or the strains in the Mo layers. Since the Si layers in these structures are amorphous, these X-ray diffraction measurements provide no information on the Si layer stresses; a complete description of the stress state in the individual layers is thus not available.

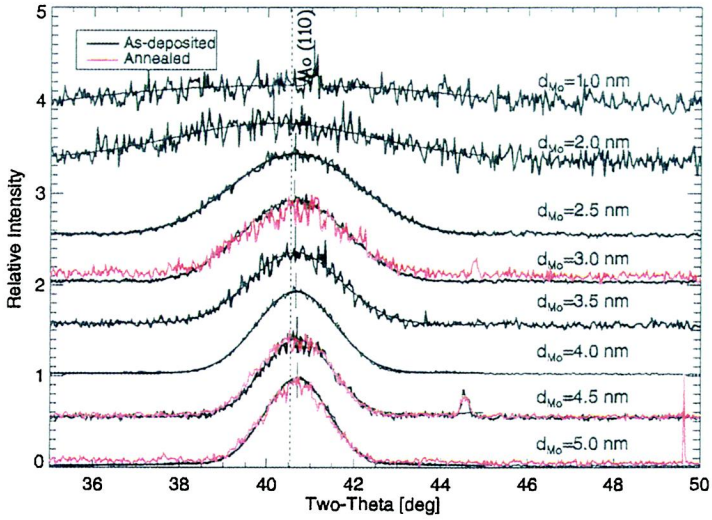

Figure 21. X-ray diffraction data for some of the Mo/Si multilayers (containing 3.0-nm-thick Si layers) shown in Figure 20.

Note that the stresses in the Mo/Si films just described depend sensitively on the deposition conditions (Ar pressure, target-to-substrate distance, background pressure, etc[18].) Consequently, the stresses reported above will not apply, in general, to Mo/Si multilayer films prepared under different conditions (i.e., in different laboratories.) To illustrate the sensitivity of multilayer film stress to one deposition condition in particular, shown in Fig. 22 are the stresses obtained in Mo/Si multilayer films as a function of background pressure, i.e., the pressure as read by the ionization gauge just prior to the introduction of the argon gas used for sputtering. The samples grown at different background

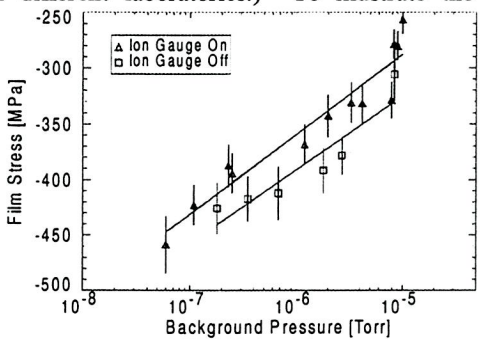

Figure 22. Stress vs. background pressure for Mo/Si multilayers.

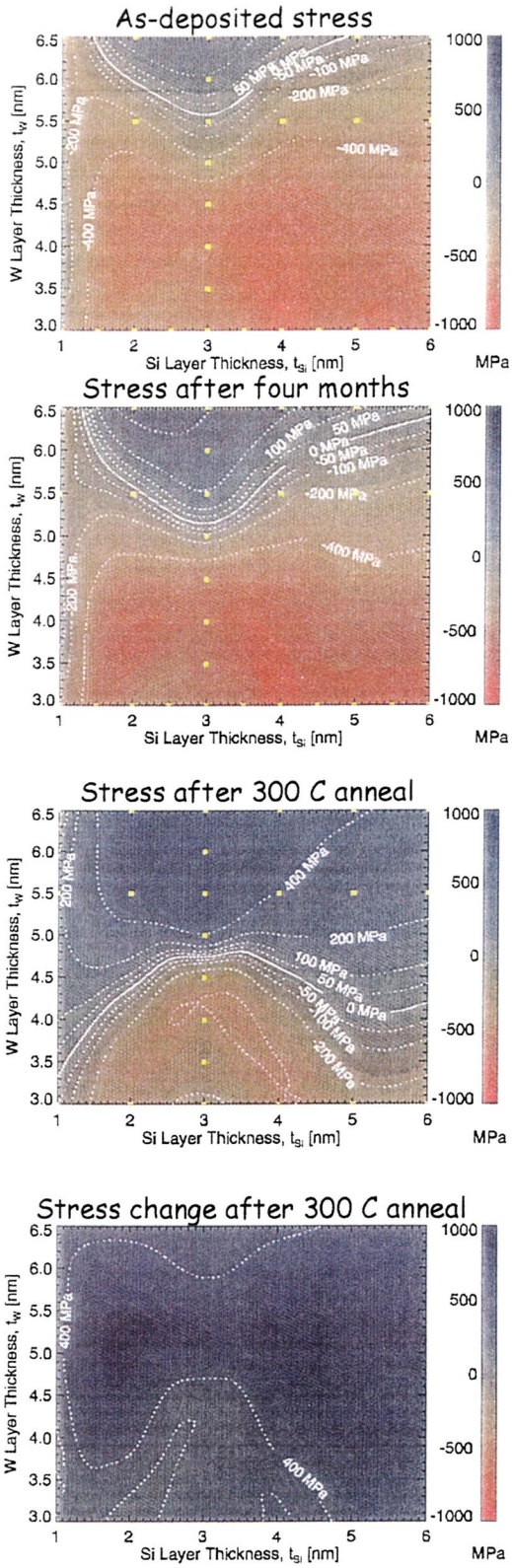

Figure 23. Stresses in W/Si multilayers.

pressures were obtained by varying the pumpdown time of the deposition system: samples grown at background pressures of order 10^{-5}-10^{-6} Torr correspond to a pumpdown times of order 1-2 hours, while samples grown in the 10^{-7} Torr pressure range correspond to pumpdown times of order 1-2 days. The stress scales linearly with the log of the background pressure, and can vary by hundreds of MPa. The stress also depends on whether or not the ion gauge is left on during pumpdown. (See reference [18] for more details.)

The dependence of stress with layer thickness as measured in W/Si periodic multilayers is even more complicated than the behavior for the Mo/Si films just described. The parametric stress maps for W/Si (analogous to those for Mo/Si shown in Fig. 20) are shown in Fig. 23, and the X-ray diffraction data in Fig. 24. The stresses in W/Si films stored in air for a period of four months change considerably, as in Mo/Si. In contrast to Mo/Si, however, the change in stress after 300 C anneal results in only positive stress change (i.e., the films become more tensile.) The X-ray data (Fig. 24) reveals that two W phases are present: the alpha phase (bcc structure) as indicated by the (110) peaks near 2θ=40.3°, as well as the beta phase (A15 structure) as indicated by the (200) peaks near 2θ=35.6°. The relative intensities of the alpha- and beta-phase peaks vary with W layer thickness, suggesting that the microstructure of these layers also varies with thickness. Furthermore, for films containing W layers thicker than about 5 nm, the beta phase is entirely consumed after 300 C anneal (or after storage in air for four months, for that matter,) but is apparently stable to thermal cycling in films containing thinner W layers.

From the data presented here, it is clear that the stress in an X-ray multilayer film is strongly dependent on the multilayer design and deposition conditions, and may vary with time even at room temperature. This fact must be considered in order to assess the effects of film stress on substrate figure.

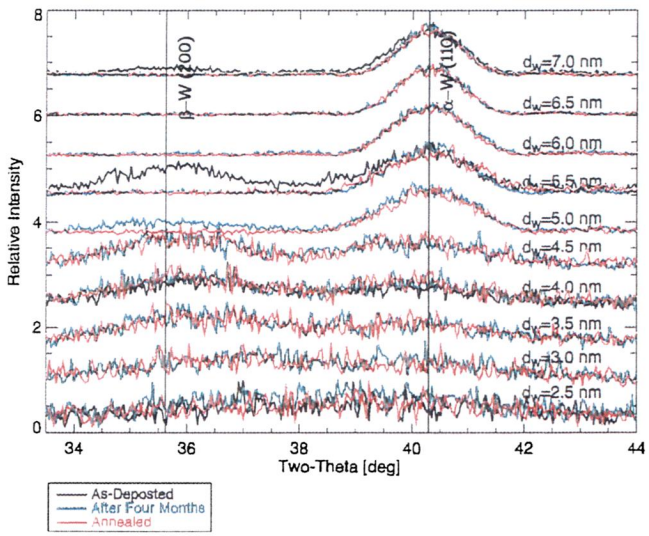

Figure 24. X-ray diffraction data for some of the W/Si multilayers (containing 3.0-nm-thick Si layers) shown in Figure 23.

6. CONCLUSION

Multilayer X-ray optics technology has matured to the point where optical systems utilizing normal incidence multilayer mirrors in the 125-300 Å region, and grazing incidence multilayers at shorter wavelengths are now practical, and are in fact finding use in a wide variety of exciting applications. I have described here some recent activities directed towards the development and further refinement of such multilayer X-ray optics. I fully expect that further advances in multilayer technology will result in a plethora of multilayer X-ray optical systems for both science and technology.

As a final topic, I would like to make explicit reference to two software packages that I have developed recently. The first, called IMD[7], computes the specular and non-specular optical properties of multilayer films, and can be used for modeling as well as curve-fitting, from the X-ray to the infrared The second, called TOPO, is used for the statistical analysis of surface roughness data, as obtained with an AFM or a WYKO instrument, for example. Both of these packages are available for downloading via the internet, at <http://www.bell-labs.com/user/windt/idl>.

ACKNOWLEDGEMENTS

I have many colleagues to thank for their various contributions to the work described above: L. Golub (SAO) for his support of the development of multilayer structures for solar physics and - along with T. Barbee (LLNL) - for providing the Mo_2C/Si TRACE mirror witness flat; F. Christensen and A. Hussein (D.S.R.I.), W. Craig, M. Stern, and C. Hailey (Columbia Univ.), and especially F. Harrison and P. Mao (Cal. Tech) for their support and their very many contributions to the development of the depth-graded multilayers for the HEFT project; W. Brown (Bell Labs) for his contributions to the work on film stress; R. Hull (Univ. of Virginia) for TEM analysis; J. Griffith (Bell Labs) for his work on surface roughness; and W. Waskiewicz for his many contributions to the multilayer research program over the years.

REFERENCES

[1] B. L. Henke, E. M. Gullikson, and J. C. Davis, *Atomic Data and Nuclear Data Tables*, Vol. **54**, No. 2, July 1993. In addition to the data contained therein, the Center For X-Ray Optics (CXRO), Lawrence Berkeley Laboratory, maintains an active database of atomic scattering factors; these data are available at <http://www-cxro.lbl.gov>.

[2] D. L. Windt, R. Hull, and W. K. Waskiewicz, *J. App. Phys.*, 71, 2675-2678 (1992)

[3] See, for example, 'The Solar Corona', L. Golub and J. M. Pasachoff, Cambridge University Press (1997)

[4] See, for example, G. Kubiak, *et al*, *J. Vac. Sci. Technol. B*, 12, 3820-3825, (1994)

[5] Delaboudinière *et al.*, *Solar Physics* **162**, 291 (1996)

[6] T.D. Tarbell, *et al.*, *Proc. 3rd SoHO Workshop*, ESA SP-373, Dec. 1994. Also see <http://vestige.lmsal.com/TRACE>.

[7] D. L. Windt, *Computers in Physics*, Jul/Aug (1998). (The IMD software can be downloaded from <http://www.bell-labs.com/user/windt/idl>.)

[8] The Center for X-Ray Optics maintains a database of measured multilayer performance, at <http:/www-cxro.lbl.gov/multilayer/survey.html>

[9] K. D. Joensen, et al., in *Multilayer and Grazing Incidence X-Ray/EUV Optics II*, R. B Hoover and A. B. C. Walker, Eds., *Proc. SPIE*, **2011**, 360-372 (1993)

[10] C. J. Hailey, *et al.*, , in *EUV, X-Ray, and Gamma-Ray Instrumentation for Astronomy VIII*, O. H. Siegmund and M. A. Gummi, Eds., *Proc. SPIE*, . **3114**, p. 535-543 (1997)

[11] W. W. Craig, et al., in *EUV, X-Ray, and Gamma-Ray Instrumentation for Astronomy IX*, O. H. Siegmund and M. A. Gummi, Eds., *Proc. SPIE*, **3445**, in press (1998)

[12] D. L. Windt and W. K. Waskiewicz, *J. Vac. Sci. Technol. B*, 12, 3826-3832 (1994)

[13] See, for example, D. G. Stearns, *J. Appl. Phys.* **65**, 491-506 (1989).

[14] D. L. Windt, W. K. Waskiewicz and J. E. Griffith, *App. Opt.*, 33, 2025-2031 (1994)

[15] D. K. G. de Boer, *Phys. Rev. B*, **51**, 5297-5305 (1995)

[16] D. K. G. de Boer, *Phys. Rev. B*, **53**, 6048-6064 (1996)

[17] 'Elements of X-Ray Diffraction', B. D. Cullity, Addison-Wesley Publishing Company (1978)

[18] D. L. Windt, W. L. Brown, C. A. Volkert, and W. K. Waskiewicz, *J. Appl. Phys.* , 78, 2423-2430 (1995)